AUT Journal of Mechanical Engineering

AUT J. Mech. Eng., 8(3) (2024) 227-240
DOI: 10.22060/ajme.2024.23148.6105

Computational Investigation of the Flow Structure and Drag Characteristics of Spheres in Accelerated Motion

Hossein Ansarian, Mostafa Hadidoolabi*

Aerospace Research Institute, Malek Ashtar University of Technology, Tehran, Iran

ABSTRACT: The unsteady motion of spheres is important for applications such as falling drops and fuel particle acceleration in nozzles. This study investigates the accelerated spheres' drag for the acceleration number -0.2 to 0.2 and the Reynolds number 20-170. Unsteady laminar Navier-Stokes equations have been solved using the finite-volume approach, dynamic structured grid, and a second-order semi-implicit pressure-based method. The steady drag coefficient range is 2.7- 0.9 for the specified Reynolds range. For the accelerating sphere, Cd values are larger than the steady-state value (For Re = 20, Cd is 6.1 for a = 125 m/s2 and 3.7 for 32 m/s2). By increasing Re, Cd decreases gradually and then tends to the steady-state value. For deceleration, Cd is smaller than the steady-state value (for Re = 20, Cd is -2.5 for a = -125 m/s2 and 1.3 for -32 m/s2). By increasing Re, Cd increases firstly, then decreases, and finally tends to the steady-state value. The larger the magnitude of acceleration, the farther away the unsteady drag curve is from the steady-state curve. When the sphere is accelerated from rest, the flowfield and the drag tend to the state of steady motion with small Reynolds. For deceleration, they tend to the state of steady motion with a large Reynolds. A new equation is proposed providing a simple accurate method for estimating the spheres' unsteady drag coefficients.

Review History:

Received: May, 02, 2024
Revised: Aug. 15, 2024
Accepted: Sep. 10, 2024
Available Online: Sep. 13, 2024

Keywords:

Sphere Drag Coefficient
Particle Acceleration
Acceleration Number
Unsteady Laminar Flow
Numerical Simulation

1- Introduction

The accuracy of the calculation of spherical particle trajectories in two-phase flows is critically affected by the equations of drag coefficient. These formulas are typically considered as functions of Reynolds number in steady flows. Many experimental data presented graphs of drag coefficient versus Reynolds number, but only for spheres in steady motion. The unsteady motion of spherical particles is more common in engineering and applications such as falling drops, fuel particle acceleration in nozzles [1], and aircraft icing. If the sphere trajectories are calculated using the steady formulas, while they experience unsteady motions, obvious deviation occurs because the drag force on spheres is not a function of the Reynolds number alone. Therefore, it is important to study the drag coefficient of spheres in unsteady motion.

Early research on the unsteady motion of spheres paid more attention to oscillating motions by theoretical methods and many experimental approaches. By theoretical analysis, Stokes [2] derived the drag of a sphere with linear small-amplitude oscillation in creeping flow. This means that the convective term was ignored, the drag consists of steady and "added mass" terms. Basset [3] showed that the forces on a sphere in unsteady low-velocity flow can be considered as the summation of steady viscous drag, added mass drag, and the effect of the history of motion. After this, a sphere's unsteady drag coefficient was generally divided into three parts to analyze. It should be noted that the convective terms in the Navier-Stokes equations were not regarded so the formula works well only for flows with low Reynolds numbers.

Since then, many estimations of unsteady drag coefficients of spheres have been developed, and the acceleration number $An = \dot{v}D/v^2$ was gradually entered into the literature. This non-dimensional parameter is defined as the ratio of local acceleration to convective acceleration. In an unsteady motion of a sphere, the local acceleration has a direct effect on the pressure distribution around the sphere so that the drag force deviates from its steady-state value. Iverson and Balent [4] stated that the drag coefficient is dependent on geometry, Reynolds number, Froude number, and acceleration number. They showed that the drag coefficient is related to the acceleration number by their experiments on circular disks moving perpendicularly in the air. Keim [5] performed experiments on cylinders rising in water and concluded that $An \geq 0.2$, the acceleration effect was obvious. Odar and Hamilton [6] got the steady drag coefficients, the added mass, and the effect of motion history, by measuring the forces on a sinusoidally oscillating sphere within the range of $0 < \mathrm{Re} < 62$. They showed the last two quantities were only functions of An.

To study the effect of spherical particle acceleration on their drag force in unsteady motion, many experiments have been

*Corresponding author's email: mhadidoolabi@mut.ac.ir

carried out, and many different results have been concluded. Roos and Willmarth [7] reported that for a sphere accelerated from zero to a constant velocity, drag exceeds the steady-state value by about 30% at high Reynolds numbers until the final quasi-steady wake is established. In contrast, Crowe [8] concluded in his theoretical study that the drag coefficient of a sphere decreases with increasing the acceleration number. Marchildon and Gauvin [9] evaluated the drag coefficients of a single solid particle moving with steady velocity, acceleration, and deceleration through still air for $103 < \mathrm{Re} < 104$. They concluded that the drag coefficient in accelerating motion was approximately the same as the steady drag, but the drag coefficient in decelerating motion was larger than the steady drag. These researchers did not reach a unit conclusion about the drag coefficient of spheres in unsteady motion. In the early experimental studies, researchers used different models, different measurement methods, and different mediums, therefore some errors may be expected. To get more accurate drag characteristics of spheres in unsteady motion, detailed flow pressure and velocity fields are needed to investigate the physical mechanisms of unsteady effects.

Moreover, some empirical formulas were given for the unsteady drag coefficient of spheres by improving the existing steady equations. Using an oscillating sphere in water, Karanfilian and Kotas [10] experimented for $102 < \mathrm{Re} < 104$ and $|An| \le 10.5$. Using statistical methods, a corrected formula $C_d = (An+1)^{1.2\pm0.03} C_{ds}$ was extracted, where C_d and C_{ds} are the unsteady and steady drag coefficients. Temkin and Kim [11] studied the motion of spheres in a shock tube for $3.2 < \mathrm{Re} < 77$, and proposed the corrected equation $C_d = C_{ds} - KA$, where K is a constant of order 1 and A is defined by $A = \left(\frac{\rho_p}{\rho} - 1\right)\frac{D}{v^2}\frac{dv}{dt}$, in which ρ is the fluid density, ρ_p is the density of the particle, v represents the relative velocity, D is the diameter of the sphere, and t is the time. Temkin and Mehta [12] conducted experiments for studying small water droplets in both decelerating and accelerating conditions with the range of $9 < \mathrm{Re} < 115$. By fitting the experimental data, they obtained the following formula of the drag coefficient:

$$\begin{cases} C_d = C_{ds} - 0.048A & (-45 < A < -3) \\ C_d = C_{ds} - \dfrac{3.829}{A} - 0.204 & (5.9 < A < 25) \end{cases} \quad (1)$$

The accuracy of experimental data is not satisfactory in the transition region $-3 \le A \le 5.9$. Tsuji et al. [13] investigated the unsteady drag characteristics of spheres with a maximum An of 0.08 and a range of Reynolds numbers from 8,000 to 16,000. They derived an empirical formula $C_d = C_{ds} + 2.7An$ that implies that the drag coefficient decreases for deceleration and increases for acceleration. To conclude, two different empirical formulas $C_d = C_{ds} + f_1(An)$ and $C_d = C_{ds} f_2(An)$, were employed, but their deviation from the experimental results was still large.

Some new research has focused on specific aspects of the spheres' drag problem. Effects of compressibility [14], high velocity [15], and surface roughness [16] have been reported. Several researchers have discussed the effect of acceleration on the spheres drag, but the role of the acceleration number has not been addressed [17, 18]. Some other works include the acceleration number in predicting the drag coefficient of the spheres, but they suggest very complicated correlations [19-22].

To summarize, acceleration has a great effect on the drag coefficient of spheres moving in the fluid. The detailed flow pressure and velocity fields around the sphere in unsteady motion are needed to understand the physical mechanism responsible for the unsteady effects. In this paper, the drag characteristics of spheres in unsteady motion are studied numerically with the Reynolds number range of 20 to 170. Firstly, the characteristics of the flow physics and drag coefficients of spheres under deceleration and acceleration conditions are analyzed. Then, a new corrected formula for the unsteady drag coefficient is proposed based on the concept of acceleration number.

2- Physical Model and Computational Method

2- 1- Physical model

A sphere with diameter D = 1 mm is placed in a still gas flow field to move with deceleration and acceleration. The absolute values of deceleration and acceleration are 32, 50, 80, 100, and 125 m/s^2. In the first set of calculations, the sphere is accelerated from rest to 2.5 m/s with constant acceleration. In the second set, it is decelerated from 2.5 m/s to rest. The Reynolds number $\mathrm{Re} = \rho v D / \mu$ ranges from 20 to 170, where ρ denotes the gas density, v denotes the relative velocity, and μ denotes the dynamic viscosity of gas.

A two-dimensional axisymmetric model is used, and the motion direction is from right to left. It is known that flow past a sphere shows to be axisymmetric and steady for Reynolds number below 200 [23]. A global moving grid [24] is applied to model the relative motion between the sphere and the surrounding fluid. In this approach, the whole computational domain (including the boundaries and internal cells) moves together with the sphere like a rigid body, i.e., the domain moves relatively to the ground. Calculation of acceleration and deceleration of the sphere is facilitated in this way. Therefore, re-meshing or mesh deformation techniques are not needed, which ensures the quality of the domain cells, enhances the numerical accuracy and saves the computation cost. Fig. 1 shows the schematics of the computational model. The computational domain is an 88D × 30D rectangle. The right, left, and top boundaries have the pressure-outlet boundary condition and the bottom line has the axisymmetric boundary condition.

The required coefficients are defined as below:

Drag coefficient $C_d = F_D / (1/2 \rho v_\infty^2 S)$,

Pressure drag coefficient $C_{dp} = F_{D_p} / (1/2 \rho v_\infty^2 S)$,

Friction drag coefficient $C_{df} = F_{D_f} / (1/2 \rho v_\infty^2 S)$,

Pressure coefficient $C_p = (p - p_\infty) / (1/2 \rho v_\infty^2)$,

Surface friction coefficient $C_f = \tau_w / (1/2 \rho v_\infty^2)$,

Where, F_D represents the total drag, F_{D_f} and F_{D_p} denote

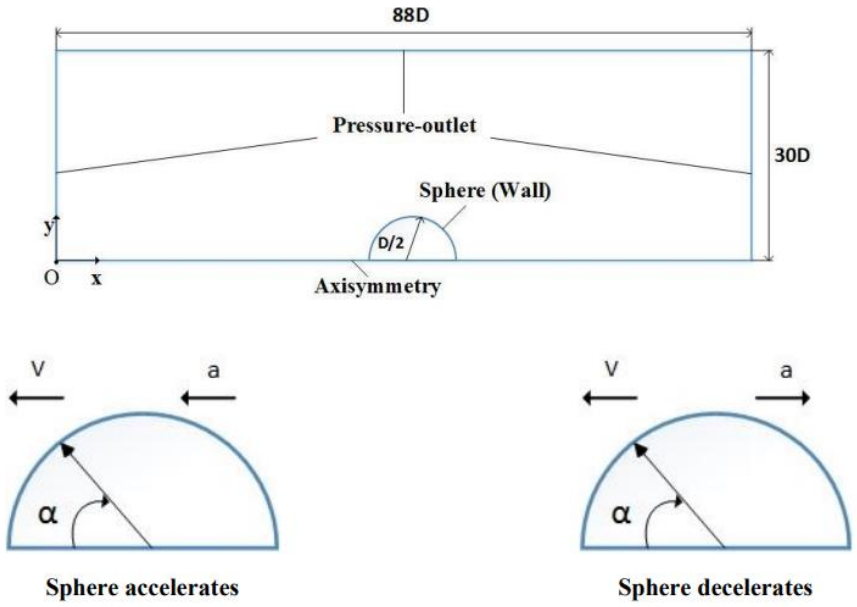

Fig. 1. Domain geometry and boundary conditions (α denotes the clockwise angle from the sphere leading edge.)

surface friction drag and pressure drag forces, v_∞ and p_∞ are free stream velocity and static pressure, S is the frontal area of the sphere, and τ_w denotes the wall shear stress on the surface.

2- 2- Numerical method

The commercial CFD software ANSYS FLUENT 19.1 has been used to solve the axisymmetric unsteady laminar incompressible Navier-Stokes equations. The governing equations are:

Continuity:

$$\nabla \cdot \mathbf{v} = 0 \tag{2}$$

Momentum:

$$\frac{\partial}{\partial t}(\mathbf{v}) + \nabla \cdot (\mathbf{vv}) = -\nabla \frac{p}{\rho} + \frac{\mu}{\rho}\nabla^2 \mathbf{v} \tag{3}$$

The Semi-Implicit Method for Pressure-Linked Equations (SIMPLE) method is applied to solve the velocity-pressure coupling. The pressure term is discretized by a second-order scheme, the diffusion terms are discretized by a second-order central difference scheme, the convection terms are discretized by a third-order MUSCL scheme, and the transient temporal terms are discretized by a first-order implicit scheme. The time step size is chosen as 10^{-5} s after the time step independence study. A structured grid is generated, which is refined near the sphere and is shown in Fig. 2. The convergence criterion is the reduction of continuity, *x*-velocity, and *y*-velocity residuals to the order of 10-5 in each time step.

2- 3- Grid Independence Study

Five sets of grids are generated for the computation, which are numbered 1-5, with the number of cells shown in Table 1. Three different values for the Reynolds number are selected to obtain the steady drag coefficients. The specific values of the results are shown in Table 1. The results from Grids 2-5 are very close, i.e. no important change is seen in the results with refining the mesh. However, the values from Grid 1 show obvious differences. Therefore, Grid 2 is selected for the main computations.

2- 4- Time Step Study and Validation of the Numerical Method

The sphere drag coefficients in the accelerated motion with $a = 100\,\mathrm{m/s^2}$ for three time steps 10^{-4} s, 10^{-5} s, and 10^{-6} s are shown in Fig. 3. As it can be seen, the results from 10^{-5} s and 10^{-6} s are almost the same, while there are large differences for the values obtained by 10^{-4} s, thus 10^{-5} s is selected as the time step size in the main unsteady simulations.

For verification, the steady flow over a sphere for a

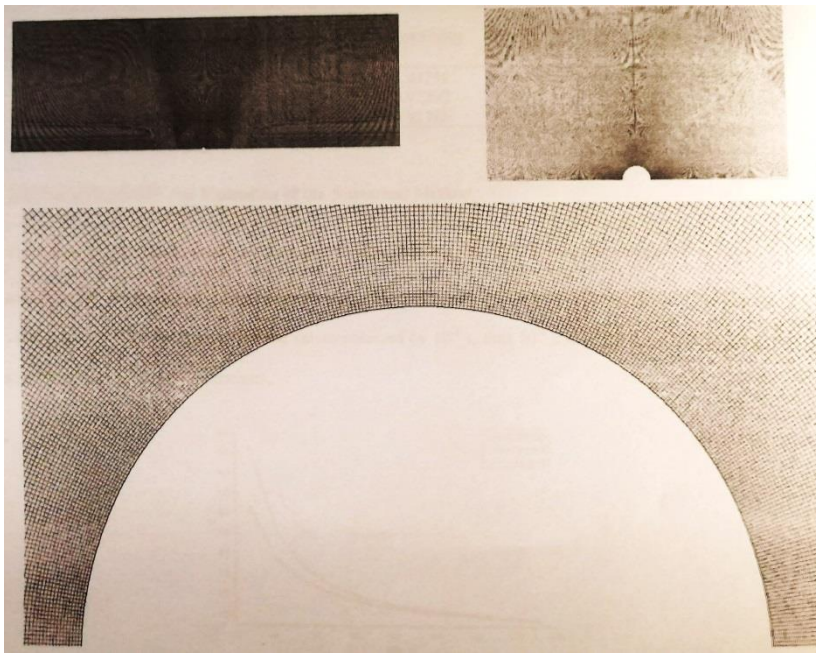

Fig. 2. Computational grid

Table 1. Grid independence study

Grid / Cd / Re	1 (215,000)	2 (470,000)	3 (645,000)	4 (875,000)	5 (1,075,000)
109.5	1.04445	1.03734	1.03759	1.03722	1.03791
123.2	0.98747	0.97827	0.97792	0.97751	0.97803
136.9	0.93933	0.92895	0.92786	0.92764	0.92788

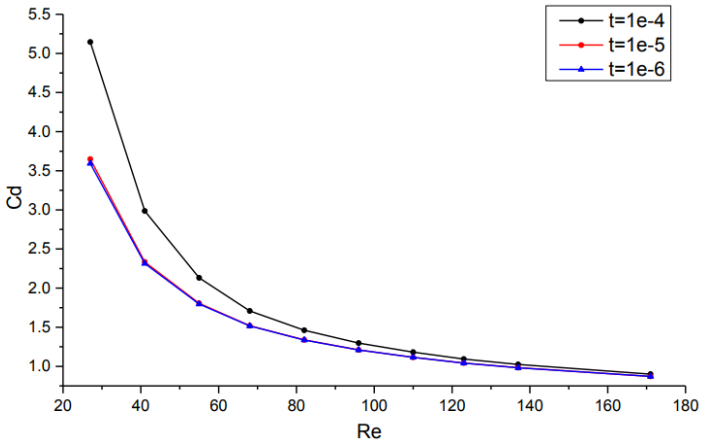

Fig. 3. Time step independence study

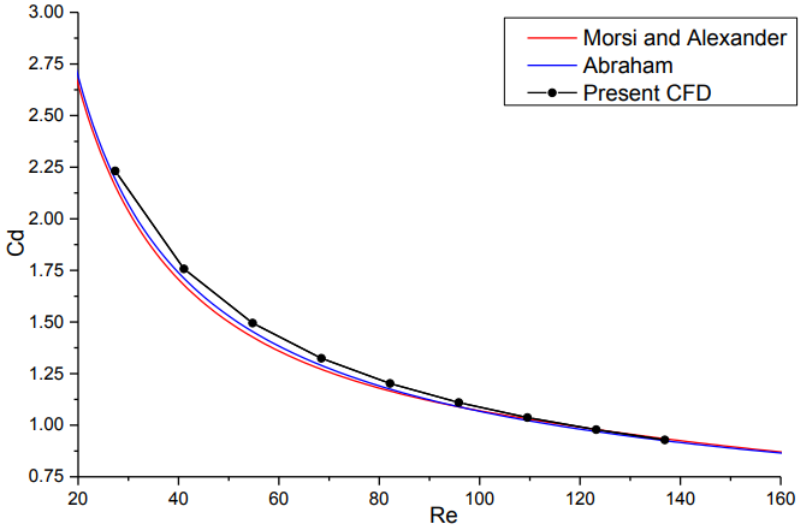

Fig. 4. Comparison of Cd values between the empirical formulas and the present CFD simulations

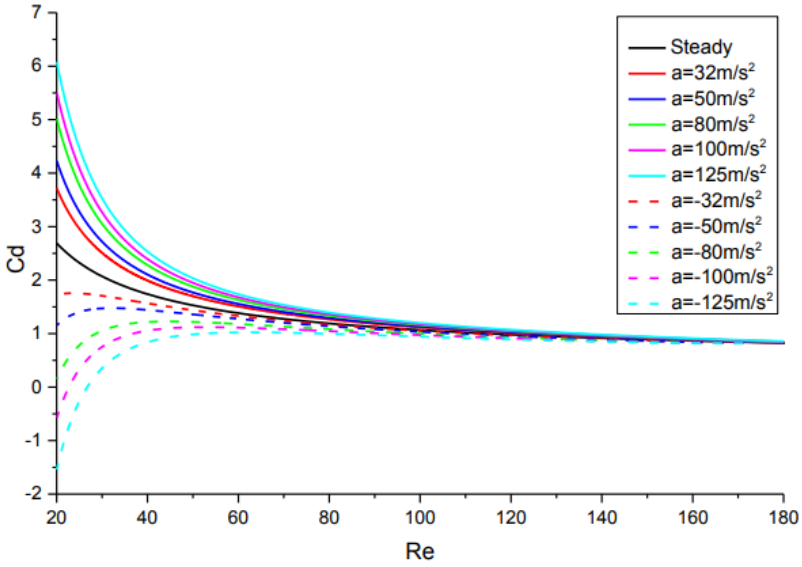

Fig. 5. Variations of sphere drag coefficients with Reynolds number for various accelerations.

Re range of 20-140 is simulated. Fig. 4 shows the drag coefficient of the present numerical study compared to the results obtained by the empirical formulas of [25] and [26]. The C_d values by the present CFD method are at most 3% higher than the empirical results, which show that CFD can calculate the sphere drag coefficients accurately.

3- Results and Discussion

3- 1- Drag properties of spheres in unsteady motion

Fig. 5 shows the drag coefficients of spheres versus the Reynolds number for different accelerations. The drag coefficient is closely correlated to the acceleration for the specified range of Reynolds number. The drag coefficients

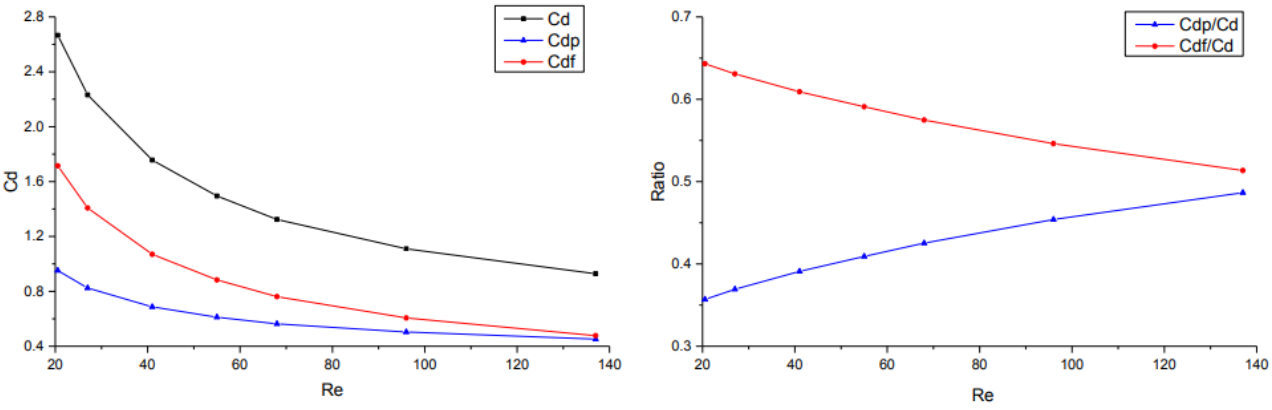

(a) Drag coefficient curves **(b) Ratios of pressure and friction drag**

Fig. 6. Variations of friction and Pressure drag coefficients in steady movement versus Reynolds number.

are significantly different for the deceleration and acceleration, the former values are smaller than the steady-state drag coefficient, while the latter values are larger. The larger the absolute value of acceleration, the unsteady drag coefficient curve is farther away from the steady-state curve. By increasing Reynolds number, the acceleration drag coefficients decrease gradually and then tend to the steady value, whereas, the deceleration drag coefficients increase firstly and then decrease, and finally tend to the steady-state value. For $\mathrm{Re}>150$, the unsteady effect is not substantial.

Fig. 6 shows the variations of pressure and frictional drag coefficients in steady movement versus Reynolds number. In the specified range of Reynolds numbers, both portions of the drags are in the same order. By increasing Re, the portion of friction drag decreases and the portion of pressure drag increases.

For the deceleration value of $a=-100\,\mathrm{m/s^2}$ and the acceleration value of $a=100\,\mathrm{m/s^2}$, the drag coefficient, the change of drag coefficient to the steady value (ΔC_d), and the ratios of the friction drag and pressure drag changes to the total change ($\Delta C_{df}/\Delta C_d$ and $\Delta C_{dp}/\Delta C_d$) are shown in Fig. 7. $|\Delta C_{dp}|$ and $|\Delta C_{df}|$ are the same order. By increasing Reynolds, the values of $|\Delta C_d|$, $|\Delta C_{dp}|$, and $|\Delta C_{df}|$ of deceleration and acceleration all decrease, $\Delta C_{dp}/\Delta C_d$ increase and $\Delta C_{df}/\Delta C_d$ decrease. A noticeable point observed in Fig. 7 is that when the sphere is decelerated at a small Re, C_{dp} and C_d has negative values i.e. that the sphere experiences a thrust force.

Fig. 8 presents the surface friction coefficient and pressure coefficient graphs for various Re values for decelerated, accelerated, and steady motions. In the steady motion, when Re increases, C_p decreases on the sphere's leading edge but it increases on the trailing edge, thus the pressure drag decreases. By increasing Re, the separation point moves upstream which results in a decrement in the region of positive shear stress. Therefore, C_f in that region is decreased, which decreases the frictional drag. It should be noted that for such low Reynolds numbers, the C_p on sphere leading edge is greater than unity. This is in agreement with the reports of [19] and [27, 28]. In the accelerated motion, the variation trend of C_p and C_f with Reynolds resembles that of the steady case. In the deceleration, there are substantial differences between high and low Reynolds numbers. For low Reynolds, the separation location moves upstream relative to the steady and accelerated motions and there is a vivid region of positive pressure close to the trailing edge. By increasing Reynolds, the separation location moves backwards and this region shrinks quickly which increases the friction and pressure drags. For higher Reynolds, this positive pressure region close to the trailing edge vanishes. By increasing the Reynolds number, C_p of the leading edge almost remains constant, and C_p of the trailing edge slightly decreases, so the pressure drag remains unchanged. By increasing the Reynolds number, the separation location is almost fixed, but the C_f decreases and causes the friction drag to decrease. Generally, increasing Remakes the drag coefficients increase at first. The coefficients then decrease and finally tend to a steady value, which is confirmed by the result of Fig. 5.

The friction and pressure coefficients of the accelerating sphere for various Reynolds numbers are shown in Fig. 9. Compared with the zero acceleration case, the acceleration causes the leading edge pressure to increase and the trailing edge pressure to decrease. The separation point is moved downstream (the separation region disappears even for low Re.) and C_f is increased in the attached flow region so that the friction and pressure drag become larger. In contrast,

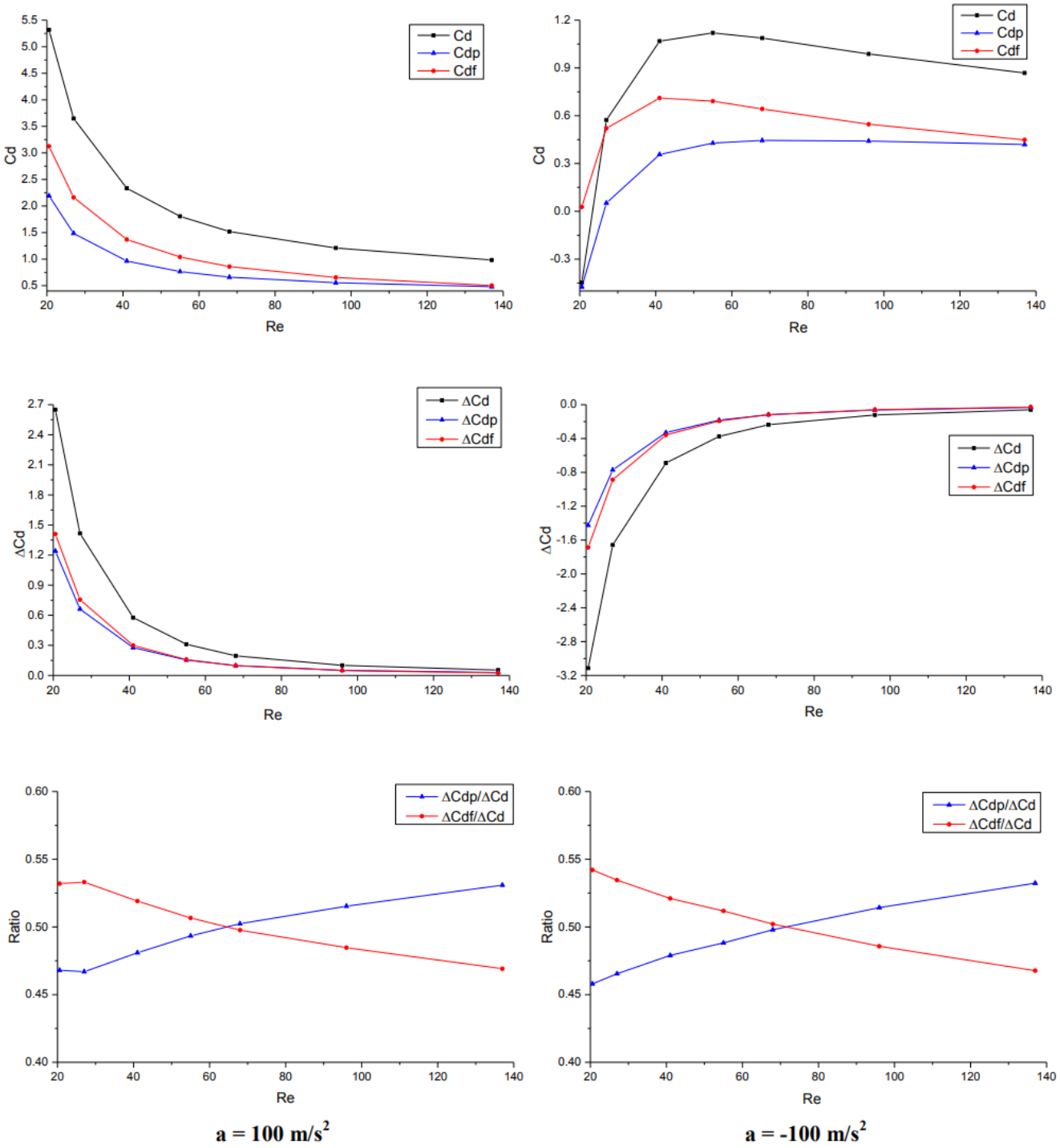

Fig. 7. Drag coefficient, change of drag coefficient to the steady value, and ratios of frictional and pressure drag changes to the total change versus Reynolds number.

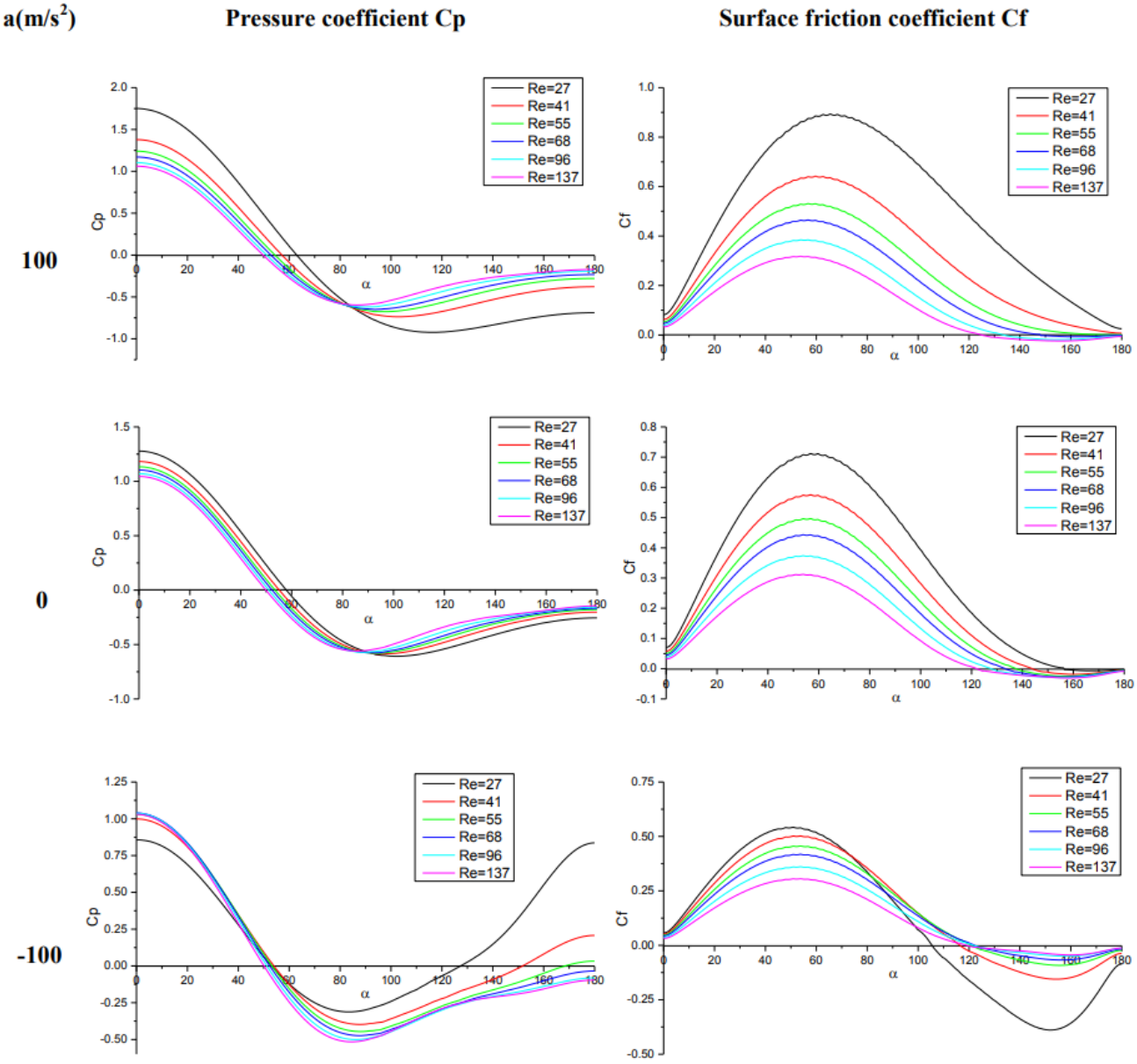

Fig. 8. Variations of pressure and surface friction coefficients over the sphere surface for different Reynolds numbers

the deceleration causes the leading edge pressure to reduce and the trailing edge pressure to increase. This leads to the forward displacement of the separation location and the decrease in the C_f in attached flow region so that the friction and pressure drag become smaller. By increasing Re, the differences in pressure and friction between the steady, decelerated, and accelerated movements gradually disappear.

The around the spheres in steady motion are shown in Fig. 10, for various Reynolds numbers. The streamlines are drawn using the relative velocity of the flow to the sphere's centroid. By increasing Re, the separation location moves upstream and the separation region grows.

The streamlines and pressure contours at $\mathrm{Re} = 68$ are shown in Fig. 11, for steady, accelerated, and decelerated motions. As the acceleration is decreased from positive to negative, the separation location moves upstream and the separation region grows. This is quite similar to the change of separation flow with the Reynolds number in the steady motion.

The ambient air is driven by the sphere during the accelerated motion. When accelerating from rest to a nominal Re, the ambient flow field pattern does not reach the steady

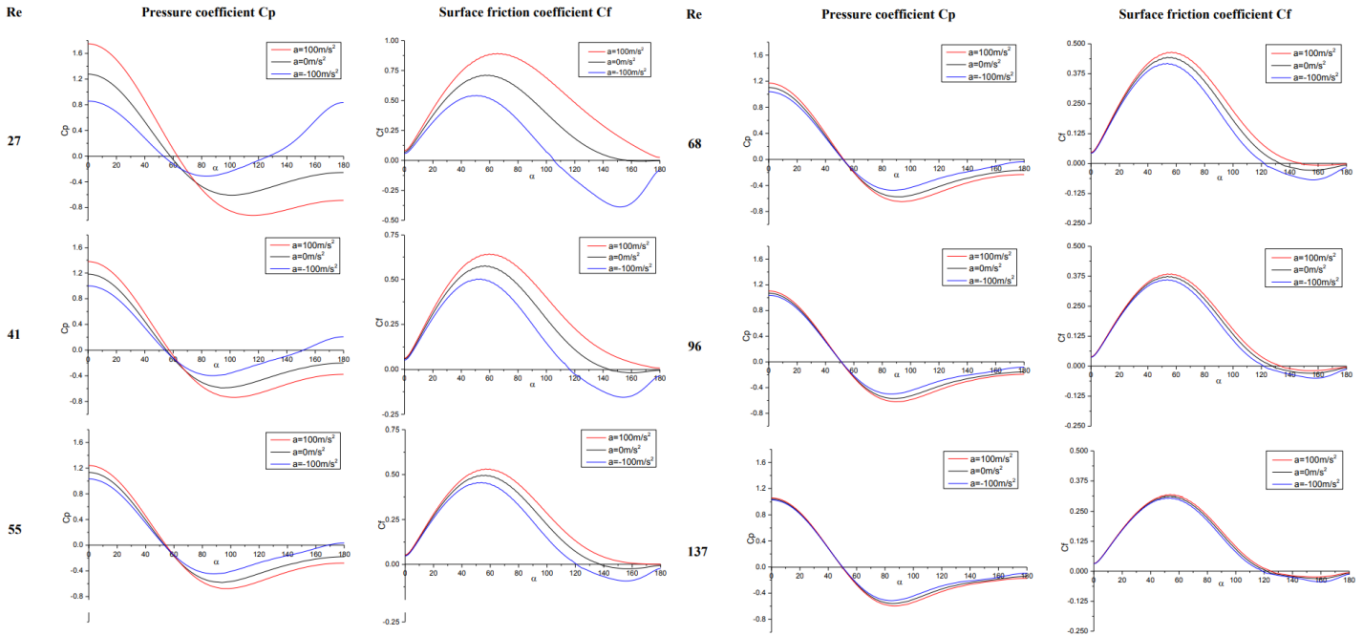

Fig. 9. Pressure coefficients and surface friction coefficients distribution for various accelerations and Reynolds numbers

state with the same Re, but it reaches the state of steady motion with a lower Re. It means a smaller separation region near the trailing edge, larger pressure on the leading edge, and smaller pressure on the trailing edge (Fig. 9). For example, the flow field pattern at $\mathrm{Re}=68$ and $a=100\,\mathrm{m/s^2}$ (Fig. 11) is similar to that of the steady case with $\mathrm{Re}=41$ (Fig. 10). This phenomenon is referred to as the "lagging effect".

Likewise, when the sphere is decelerated from a high to a nominal Re, due to the lagging effect, the airflow field pattern around the sphere and the surface friction and pressure coefficients tend to the pattern of the steady case with a higher Re. A larger separation region is formed near the trailing edge, the leading edge pressure is smaller, and the trailing edge pressure is larger (Fig. 9). For example, the flow field pattern at $\mathrm{Re}=68$ and $a=-100\,\mathrm{m/s^2}$ (Fig. 11) is similar to that of steady motion with $\mathrm{Re}=137$ (Fig. 10).

It can be concluded that compared with the drag force in the steady motion, the drag force of the deceleration motion is smaller and the drag force of the acceleration motion is larger because of the lagging effect. This conclusion is similar to that of Roos and Willmarth [7], and Tsuji [13], while the results presented by Marchildon and Gauvin [9] give almost the opposite conclusion. It is possible that some uncertainty existed in the early experiments, and the airflow field was not measured correctly. The present CFD simulation provides a detailed flow structure and pressure and surface friction coefficient distributions to discuss the drag characteristics in unsteady motion.

3- 2- Modified equation for drag coefficient

To accurately compute the motion of spherical particles in multi-phase flows, a general formula for the drag coefficient of spheres should be developed, which gives satisfactory results for steady and unsteady motions. Several empirical expressions have been introduced so far, such as the equations suggested by Karanfilian and Kotas [12], Temkin and Mehta [14], and Tsuji [15]. In general, two different empirical equations, $C_d=C_{ds}+f_1(An)$ and $C_d=C_{ds}f_2(An)$, were proposed, but they still have large deviations from the results.

Here, two types of formulas are developed for the drag coefficient based on the CFD results of steady and accelerated motion. Both drag coefficients are functions of the Acceleration number and Reynolds number.

$$C_d=\left(\lambda An+\beta\right)^{\delta}C_{ds} \tag{4}$$

$$C_d=C_{ds}+kAn+l \tag{5}$$

Here, the parameters, λ, β, k, δ, and l are derived from the least squares method, C_d is the unsteady drag coefficient, C_{ds} is the steady drag coefficient which is a function of Re. The parameters l and λ are used for the first time. The steady drag coefficient $C_{ds}=0.29238\left(1+9.06/\sqrt{\mathrm{Re}}\right)^2$ is adopted by Abraham's result [26]. The final equations are as

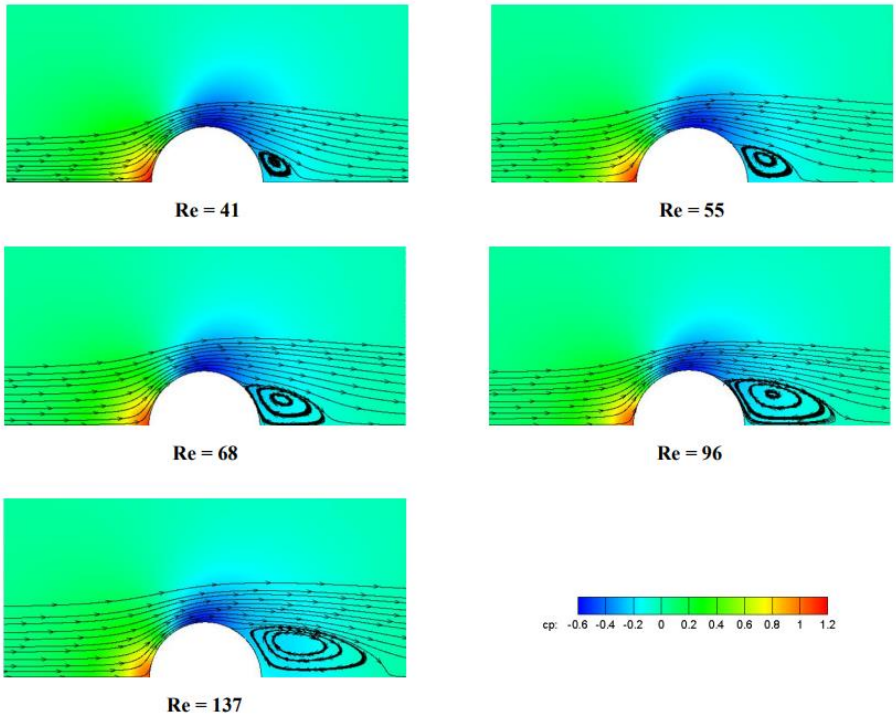

Fig. 10. Streamlines and pressure contours over the spheres in steady motion for various Reynolds numbers

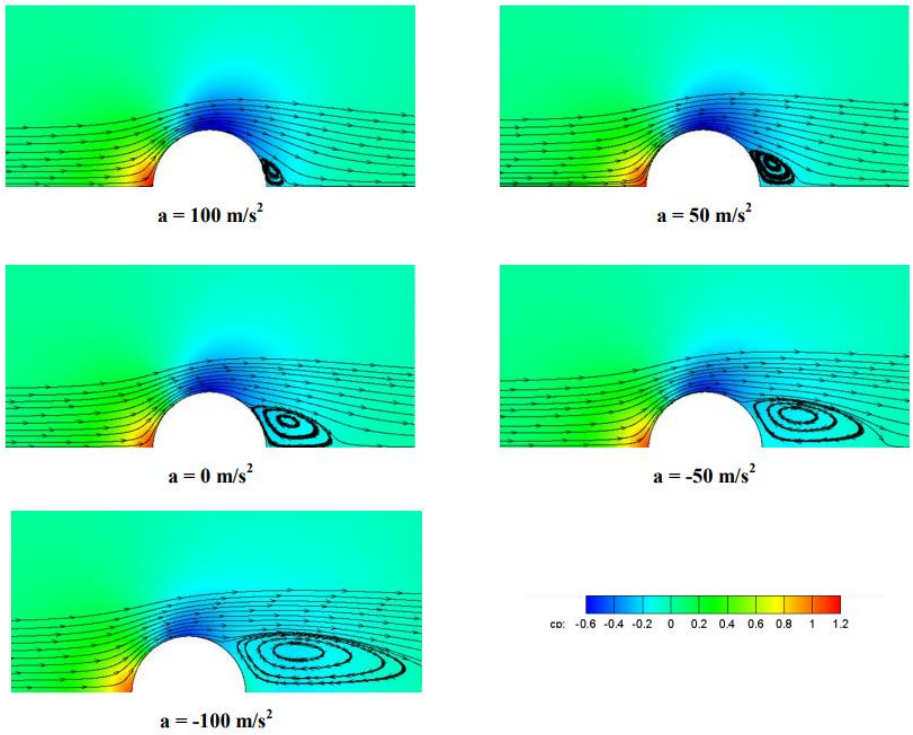

Fig. 11. Streamlines and pressure contours over the spheres at Re = 68 for various accelerations

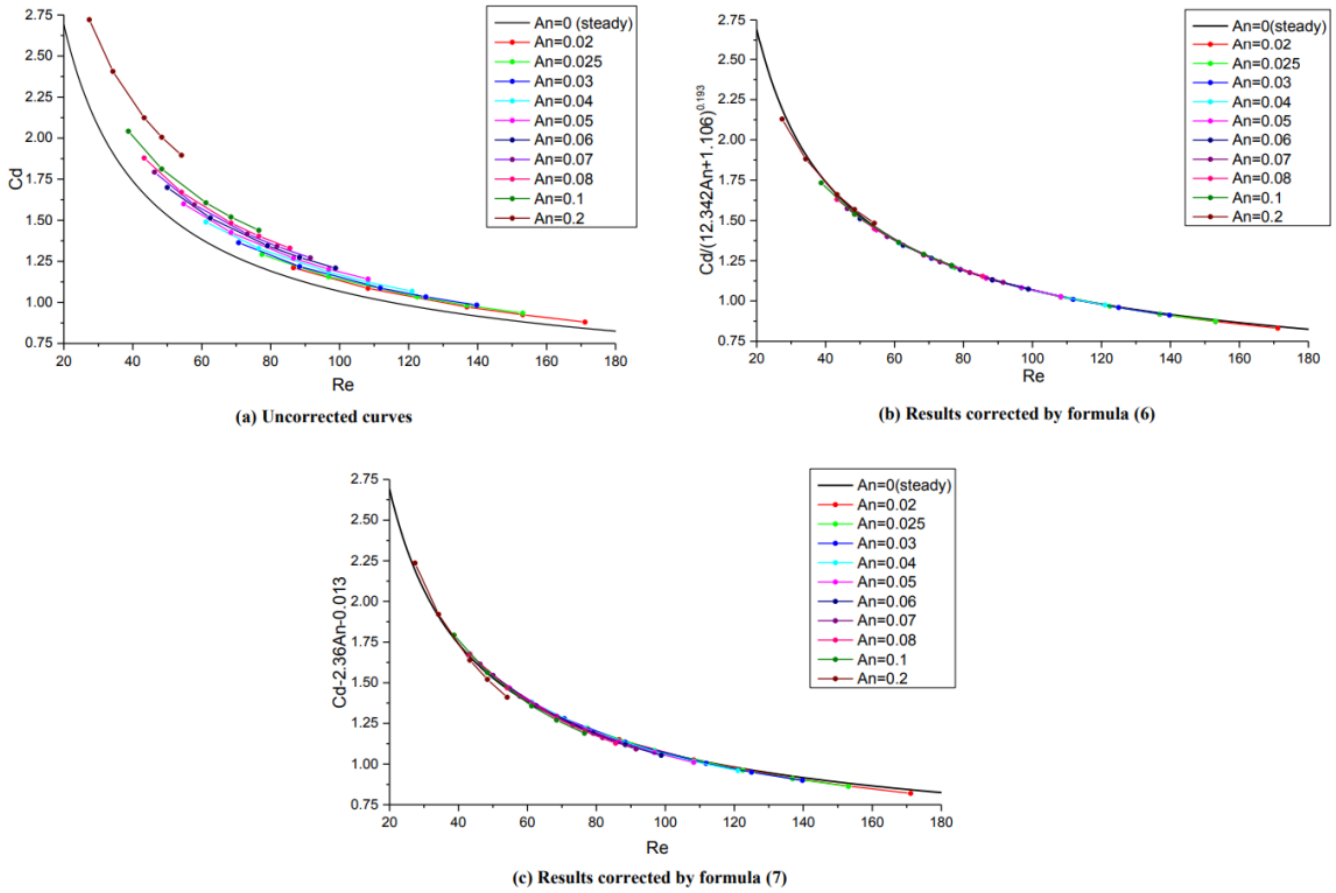

Fig. 11. Streamlines and pressure contours over the spheres at Re = 68 for various accelerations

below:

$$\begin{cases} C_d = \left(12.342An + 1.106\right)^{0.193} C_{ds} & \left(0.02 \le An \le 0.2\right) \\ C_d = \left(0.735An + 0.996\right)^{1.794} C_{ds} & \left(-0.2 \le An \le -0.02\right) \end{cases} \quad (6)$$

$$\begin{cases} C_d = C_{ds} + 2.36An + 0.013 & \left(0.02 \le An \le 0.2\right) \\ C_d = C_{ds} + 2.25An + 0.026 & \left(-0.2 \le An \le -0.02\right) \end{cases} \quad (7)$$

Fig. 12 shows the graphs of the drag coefficient versus the Reynolds number for the acceleration case of $An > 0$. The raw data, and corrected data by Eqs. (6) and (7) are shown in the figure. Similar curves for the deceleration of $An < 0$, are shown in Fig. 13.

In the selected ranges of Acceleration number and Reynolds number, Eq. (6) gives better results for the accelerated motion, and Eq. (7) gives better results for the decelerated motion. Therefore, the final corrected formulas of the sphere drag coefficient are proposed as follows:

$$\begin{cases} C_d = \left(12.342An + 1.106\right)^{0.193} C_{ds} & \left(0.02 \le An \le 0.2\right) \\ C_d = 2.25An + 0.026 + C_{ds} & \left(-0.2 \le An \le -0.02\right) \end{cases} \quad (8)$$

4- Conclusion

The numerical simulation of spheres in the unsteady motion has been carried out to study the drag characteristics, where the Reynolds number ranges from 20 to 170 and the Acceleration number ranges from -0.2 to 0.2. Several conclusions are obtained.

1) The steady drag coefficient ranges from 2.7 to 0.9 for the specified Reynolds number range. For the accelerating sphere, the drag coefficient values are larger than the steady values (C_d = 6.1 for Re = 20, a = 125 m/s^2 and C_d = 3.7 for Re = 20, a = 32 m/s^2). By increasing the Reynolds number, they decrease gradually and then tend to the steady-state value. For the decelerating sphere, the drag coefficient values are smaller than the steady values (C_d = -2.5 for Re = 20, a = -125 m/s^2 and C_d = 1.3 for Re = 20, a = -32 m/s^2). By increasing Reynolds number, they increase firstly and then decrease, and finally tend to the steady-state value. The larger the absolute

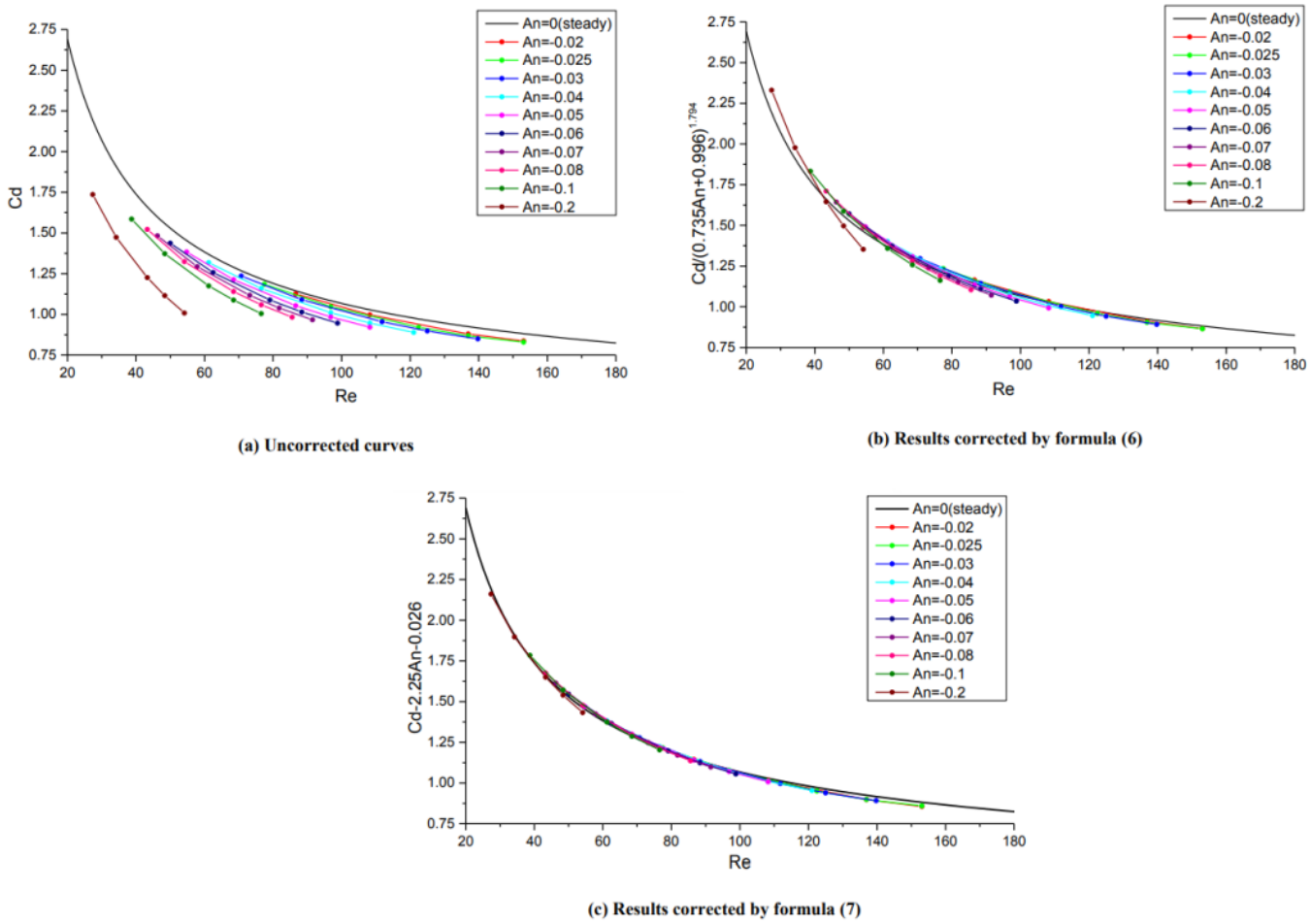

(a) Uncorrected curves

(b) Results corrected by formula (6)

(c) Results corrected by formula (7)

Fig. 13. Drag coefficients as a function of Re for An < 0

value of acceleration, the farther away the unsteady drag coefficient curve is from the steady-state curve.

2) An obvious lagging effect is observed in the unsteady motion with a small Reynolds number. When a sphere accelerates from rest to a nominal Reynolds number, the flow field structure around the sphere, the pressure and surface friction coefficients, and the total drag coefficient tend to the case of steady motion with a smaller Reynolds number. When the sphere decelerates from a high velocity to a nominal Reynolds number, these parameters tend to the state of steady motion with a larger Reynolds number.

3) Based on the numerical simulation results, a corrected formula of unsteady drag coefficient for spheres is proposed within the present ranges of Reynolds numbers and Acceleration numbers. The proposed formula showed good agreement with the previous empirical data. For future works, similar formulas may be derived for the drag coefficient of the spheres in compressible flows and turbulent flows.

Nomenclature

a	Acceleration, m/s^2
An	Acceleration number
C	Aerodynamic coefficient
D	Diameter, m
F	Force, N
g	Gravitational acceleration, m/s^2
p	Pressure, Pa
Re	Reynolds number
S	Frontal area, m^2
t	Time, s
$\mathbf{v}$	Velocity vector, m/s
v	Relative velocity, m/s
x, y	Cartesian coordinates

Greek Symbols

μ	Viscosity, N.s/m^2
ρ	Density, kg/m^3

τ Shear stress, Pa

λ, β, k, δ, l Least squares parameters

Subscript

d drag

ds steady drag

f friction

p Pressure, particle

w wall

∞ Free-stream condition

References

[1] B. Jalili, P. Jalili, Numerical analysis of airflow turbulence intensity effect on liquid jet trajectory and breakup in two-phase cross flow, Alexandria Engineering Journal, 68 (2023) 577-585.

[2] G.G. Stokes, On the effect of the internal friction of fluids on the motion of pendulums, Transactions of the Cambridge Philosophical Society, 9(1) (1850), 1-85.

[3] A.B. Basset, On the motion of a sphere in a viscous liquid, Philosophical Transactions of the Royal Society A, 179(1) (1888) 43-63.

[4] H.W. Iversen, R. Balent, A correlating modulus for fluid resistance in accelerated motion, Journal of Applied Physics, 22(3) (1951) 324-328.

[5] S.R. Keim, Fluid resistance to cylinders in accelerated motion, Journal of Hydraulic Engineering, 82(6) (1956) 1-14.

[6] F. Odar, W.S. Hamilton, Forces on a sphere accelerating in a viscous fluid, Journal of Fluid Mechanics, 18(2) (1964) 302-314.

[7] F.W. Roos, W.W. Willmarth, Some experimental results on sphere and disk drag, AIAA Journal, 9(2) (1971) 285-291.

[8] C.T. Crowe, Drag coefficients of inert, burning, or evaporating particles accelerating in gas streams, PhD Thesis, University of Michigan (1961).

[9] E.K. Marchildon, W.H. Gauvin, Effects of acceleration, deceleration and particle shape on single-particle drag coefficients in still air, Aiche Journal 25(6) (1979) 938-948.

[10] S.K. Karanfilian, T.J. Kotas, Drag on a sphere in unsteady motion in a liquid at rest, Journal of Fluid Mechanics, 87(1) (1978) 85-96.

[11] S.I. Temkin, S.S. Kim, Droplet motion induced by weak shock waves, Journal of Fluid Mechanics, 96(1) (1980) 133-157.

[12] S.I. Temkin, H.K. Mehta, Droplet drag in an accelerating and decelerating flow, Journal of Fluid Mechanics, 116(1), (1982) 297-313.

[13] Y. Tsuji, N. Kato, T. Tanaka, Experiments on the unsteady drag and wake of a sphere at high Reynolds numbers, International Journal of Multiphase Flow, 17(3) (1991) 343-354.

[14] M. Khalloufi, J. Capacelatro, Drag force of compressible flows past random arrays of spheres. International Journal of Multiphase Flow, 165(8) (2023).

[15] E. Loth, J.T. Daspit, M. Jeong, T. Nagata, T. Nonomura, Supersonic and hypersonic drag coefficients for a sphere, AIAA Journal, 59(8) (2021) 3261-3274.

[16] S.D.J.S. Nanayakkara, J. Zhao, S.J. Terrington, M.C. Thomson, K. Hourigan, Effects of surface roughness on the drag coefficient of spheres freely rolling on an inclined plane, Journal of Fluid Mechanics, 984(A13) (2024) 1-41.

[17] H. Kalman, D. Portnikov, New model to predict the velocity and acceleration of accelerating spherical particles, Powder Technology, 415 (2023).

[18] P.K. Billa, T. Josyula, C. Tropea, P.S. Mahapatra, Motion of a rigid sphere entering and penetrating a deep pool, Journal of Fluid Mechanics, (2024).

[19] S. Zhou, G. Zhang, X. Xu, C. He, Experiments on the drag coefficient of a sphere with a variable velocity, Water Supply, 23(5) (2023) 1903-1916.

[20] N. Singh, M. Kroells, C. Li, E. Ching, M. Ihme, C. Hogan, T. Schwartzentruber, A general drag coefficient for flow over a sphere, Journal of Fluid Mechanics, (2020).

[21] S. Davey, C. Atkinson, J. Soria, Measuring unsteady drag of the flow around a sphere based on time series displacement measurements using physics-informed neural networks, Experimental Thermal and Fluid Science, 144 (2023).

[22] L. Unglehrt, M. Manhart, Decomposition of the drag force in steady and oscillatory flow through a hexagonal sphere pack, Journal of Fluid Mechanics, 974 (A32) (2023) 1-36.

[23] T.A. Johnson, V.C. Patel, Flow past a sphere up to a Reynolds number of 300, Journal of Fluid Mechanics, 378 (1999) pp. 19-70.

[24] Q. Qu, M. Hu, H. Guo, P. Liu, R.K. Agarwal, Study of ditching characteristics of transport aircraft by global moving mesh method, Journal of Aircraft, 52(5) (2015) 1550-1558.

[25] S.A. Morsi, A.J. Alexander, An investigation of particle trajectories in two-phase flow systems, Journal of Fluid Mechanics, 55(2) (1972) 193-208.

[26] F.F. Abraham, Functional dependence of drag coefficient of a sphere on Reynolds Number, Physics of Fluids, 13(8) (1970) 2194-2195.

[27] J. Magnaudet, M. Rivero, J. Fabre, Accelerated flows past a rigid sphere or a spherical bubble. I: Steady straining flow, Journal of Fluid Mechanics, 284(1) (1995) 97-135.

[28] F. Liu, P. Liu, Q. Qu, L. Lin, T. Hu, Numerical study of flow physics and drag of spheres in unsteady motion, in: 2018 Fluid Dynamics Conference, 2018, Georgia, USA, 2018.

HOW TO CITE THIS ARTICLE
H. Ansarian, M. Hadidoolabi, Computational Investigation of the Flow Structure and Drag Characteristics of Spheres in Accelerated Motion, AUT J. Mech Eng., 8(3) (2024) 227-240.

DOI: 10.22060/ajme.2024.23148.6105